







Microtextural, spectroscopic, and chemical characterization of amazonite from the Serra Branca Pegmatite, Northeastern Brazil

Glenda Lira Santos^{1*} , Sandra de Brito Barreto¹ , Igor Manoel Belo de Albuquerque e Souza¹ , José Ferreira de Araújo Neto¹ , Luis Sánchez-Muñoz² , Lauro César Montefalco de Lira Santos¹ 

Abstract

The Serra Branca pegmatite in northeastern Brazil is unique because of its megacrysts of bluish-green amazonite currently exploited for ornamental purposes and as high-quality gemstones. Here we analyze microtextural, spectroscopic, and geochemical data on specimens from two magmatic generations of amazonite from this pegmatite in order to characterize their mineralogy and propose a schematic evolution diagram for twinning during their development. The amazonite consists of intergrowths of the low microcline and low albite XRD varieties that evolved according to a twin coarsening process, in which the first generation (I-tg) of $\pm A/P$ twinning developed at the monoclinic-triclinic transformation, whereas the second generation (II-tg) gave rise mainly to $\pm A$ twins. The bluish-green color of the amazonite was preserved during the process of microcline twinning. In addition to the irrational II-tg twinning, which is typically found in microcline from anorogenic settings, the serra branca amazonite crystals also show elevated contents of Rb, Pb, Fe, Cs, and Tl in both generations, whereas albitic intergrowths present high concentrations of Fe, Pb, Sr, and Ga. Finally, our chemical and spectroscopic results are compatible with the hypothesis that Pb-water centers account for the bluish green color in amazonite.

KEYWORDS: Serra Branca amazonite pegmatite; anorogenic pegmatite; twin evolution; spectroscopy; geochemistry.

INTRODUCTION

Alkali feldspar has long been used to investigate pegmatite evolution due to their chemical characteristics that provide unique constraints on its crystallization history (Foord and Martin 1979, Abad-Ortega *et al.* 1993, Larsen 2002, Alfonso *et al.* 2003, Brown *et al.* 2017). Detailed microtextural characterization, including the perthitic intergrowths, has been applied to provide additional insights on crystal growth, cooling rates, and coarsening and/or replacement reactions with late magmatic or external aqueous fluids (Parsons *et al.* 2015).

Amazonite is a bluish green variety of K-feldspar (microcline or orthoclase) that has been the focus of mineralogical studies since the early 19th century (Ostrooumov 2016). Most previous studies focused on the origin of the blue-green

color, atomic structure, and H₂O content (Hofmeister and Rossman 1985, Beran 1986, Ostrooumov 2016). However, its microtextural investigation is still limited, as most studies apply a descriptive approach (Nakano and Makino 2010 and references therein).

The majority of the amazonite occurrences are concentrated in granitic pegmatites, being an earmark of the niobium-yttrium-fluorine (NYF) pegmatite type (Martin *et al.* 2008). Typically, it occurs as microcline (Hofmeister and Rossman 1985, Martin *et al.* 2008, Ostrooumov 2016), frequently composed of twin patterns and albite exsolution. This texture appears when monoclinic (C₂/m) to triclinic (C $\bar{1}$) transition occurs, turning sanidine (C₂/m) into microcline (C $\bar{1}$) (Sánchez-Muñoz *et al.* 2008). The loss of the mirror plane (m) and the binary axis (2) from the C₂/m to C $\bar{1}$ transformation gives the four orientations variants (i.e., A+, A-, P+, and P-) that can be explained by the Albite (A) and Pericline (P) twin laws. The Pericline law has [010] as twin axis, and the Albite law is defined as a reflection across the (010) plane, resulting in two twins A+ and A- in contact along a (010) twin boundary (Sánchez-Muñoz *et al.* 2012). The development of twinning in granitic pegmatites forms different types of cross-hatched microstructures, such as tartan, parquet, and chessboard, which are originated from “stress centers” at the contact with other minerals (e.g., albite films, diamond-shaped albites; Sánchez-Muñoz *et al.* 2012). Sánchez-Muñoz *et al.* (2012) described that the twin development in granitic pegmatites most likely occurs according to the avalanche-like

Supplementary data

Supplementary data associated with this article can be found in the online version: <http://sfbjg.siteoficial.ws/Sf/2022/488920220210072.pdf>.

¹Departamento de Geologia, Centro de Tecnologia e Geociências, Universidade Federal de Pernambuco – Recife (PE), Brazil. E-mails: glendaliraa@gmail.com, sandradebritobarreto@gmail.com, igor.manoel.belo@gmail.com, araujoneto.geo@gmail.com, lauro.lsanos@ufpe.br

²Department of Geology, National Museum of Natural Sciences – Madrid, Spain. E-mail: lsm@mncn.csic.es

*Corresponding author.



events with self-organization capabilities. In this process, the Albite and Periclone twins evolve freely during the subsolidus stage forming different patterns until reach a “barrier” such as a perthitic vein, where they stop developing.

Despite their good quality for the ornamental rock industry, few occurrences of amazonite in northeastern Brazil are reported, being mostly associated with dykes or veins. The main examples are the Serra do Pinheiro (Pernambuco; Lira Santos *et al.* 2017), Serra da Maturagem (Ceará; Prado *et al.* 1980), and Tenente Ananias pegmatitic field (Rio Grande do Norte State; Barreto 1991). Recent discoveries of remarkable amazonite mineralization in pegmatites from the Borborema Province in NE Brazil brought attention to the first occurrence of NYF pegmatites in the region, located at the Vieirópolis Pegmatite Field (Lira Santos *et al.* 2020). The main occurrence is the megacrystic amazonite Serra Branca pegmatite, in the Amazon Mine from the Granistone Company, which differs from the Alto Serra Branca pegmatite from Pedra Lavrada where the serrabrancaite was first described (Witzke *et al.* 2000). This pegmatite body is traded in large blocks (Fig. 1A) to be used as ornamental material as seen in shopping malls in NE Brazil (Fig. 1B). In addition, at the mine tailings, there are also amazonite grains that can be used as gemological ornaments (Fig. 1C).

To first characterize the amazonite from the Serra Branca pegmatite, this article explores microtextural, spectroscopic, and geochemical aspects of the amazonite crystals to provide new insights on the amazonite typomorphic characteristics

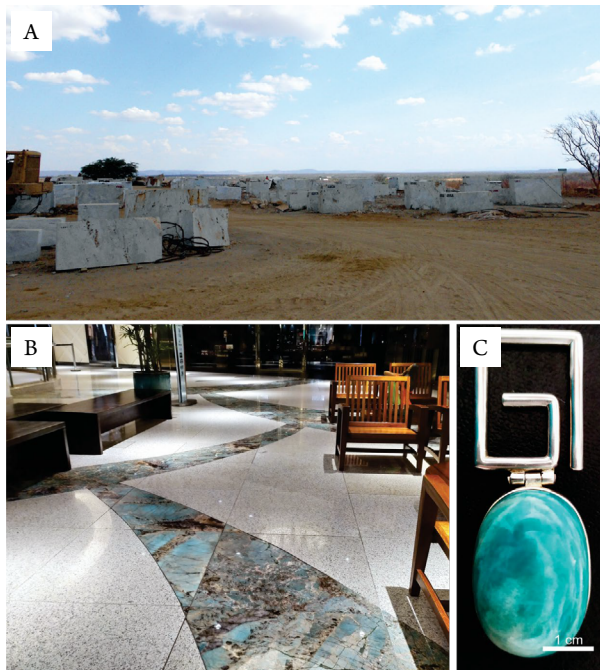


Figure 1. Amazonite economic context: (A) Blocks patio in the Amazon Mine where the amazonite blocks are stored and traded by the Granistone Company; (B) The ornamental rock tiles from the Serra Branca amazonite pegmatite on the main hall of the RioMar Shopping Mall (Recife City, Pernambuco State); (C) Serra Branca amazonite jewelry ornamented with silver, designed by Sandra Brito.

and suggest a schematic evolution diagram for the development of its twinning pattern.

GEOLOGICAL SETTING

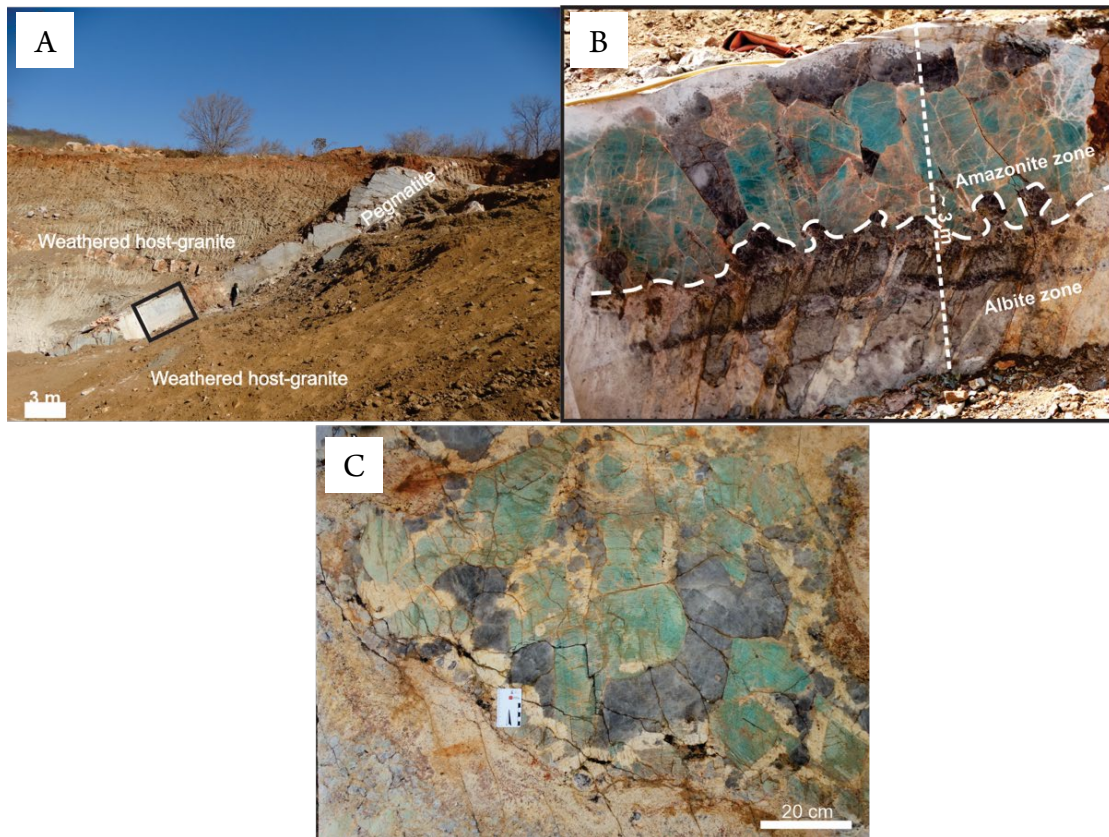
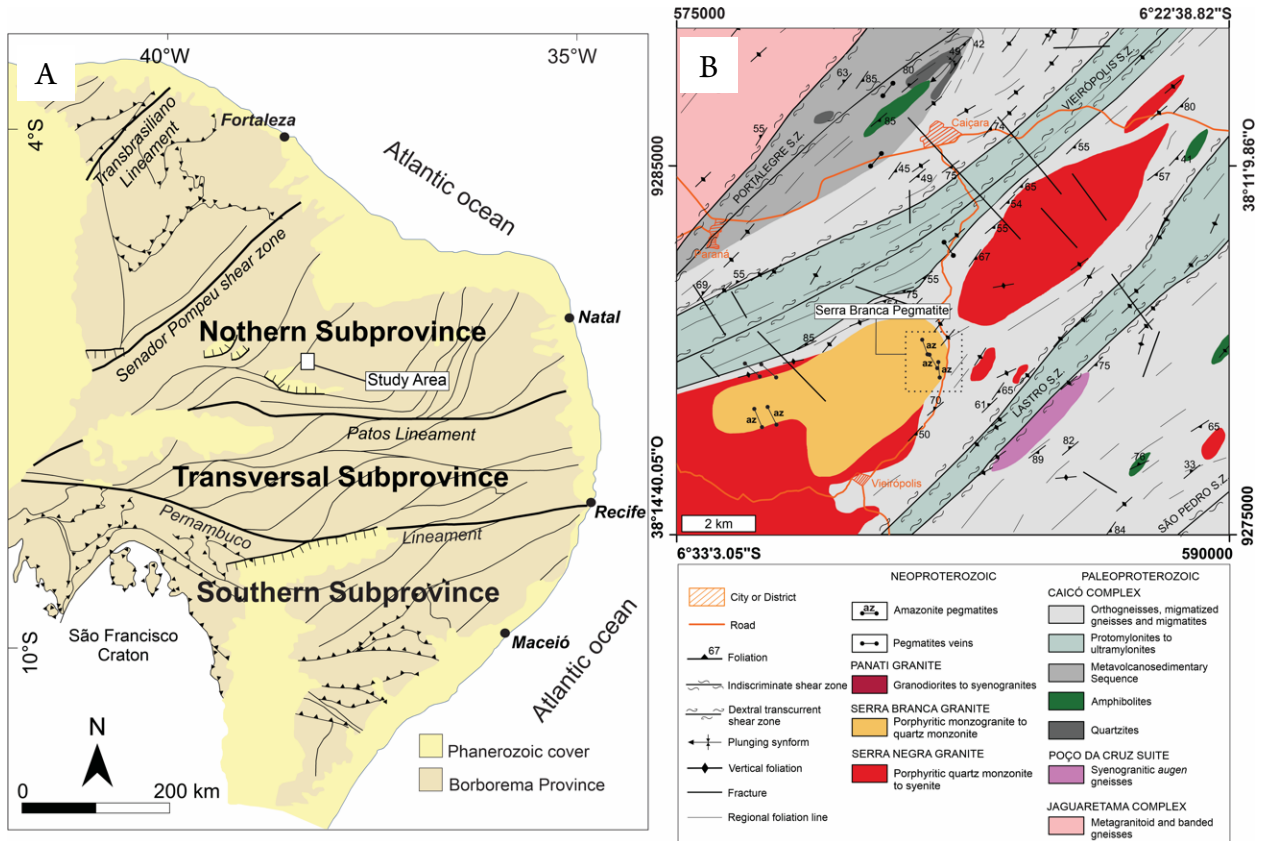
The Serra Branca amazonite pegmatite is located in the Vieirópolis Pegmatite Field (Lira Santos *et al.* 2020), in the context of the Rio Piranhas-Seridó Terrane of the Borborema Province (Fig. 2A). The region occupies part of the Northeastern South American platform, as a result of compressive deformation during the Brasiliano Orogeny (ca. 650–500 Ma) (Almeida *et al.* 1981, Brito Neves *et al.* 2014). This province is commonly divided into Northern, Transversal, and Southern subprovinces, which are bounded by the Patos and Pernambuco strike-slip lineaments (Van Schmus *et al.* 2008). The lithological framework of the Rio Piranhas-Seridó Terrane encompasses Paleoproterozoic medium- to high-grade metamorphic rocks including migmatitic and gneissic sequences as well as amphibolites and metasedimentary lithotypes (Souza *et al.* 2007, Medeiros *et al.* 2012). In the study area, widespread plutonic rocks outcrop, being possibly sin-kinematic with the Lastro and Vieirópolis strike-slip shear zones, where medium-grained monzogranite to quartz monzonite from the Serra Branca Granite occurs, hosting the studied pegmatitic bodies (Fig. 2B; Araújo Neto *et al.* 2018, Souza *et al.* 2020b).

The Vieirópolis Pegmatite Field has several pegmatite dykes, which are hosted by the Serra Branca Granite, including the Serra Branca amazonite pegmatite, being the main body mineralized in megacrystic amazonite and focus of this article (Lira Santos *et al.* 2020, Souza *et al.* 2020b). The Serra Branca amazonite pegmatite consists of two similar NW-trending tabular bodies ~3 m thick (Fig. 3A). This pegmatite is uncommonly zoned, with an amazonite-rich zone (ca. 70% vol.) mainly concentrated in the middle and top, and an albite-rich zone at the bottom and sometimes penetrating the amazonite-rich zone (Fig. 3B).

The amazonite-rich zone is composed of amazonite and grayish quartz as the dominant minerals, while biotite, helvite, galena, ilmenite, aikinite, chalcocite, hematite, magnetite, columbite-(Mn), phenakite, titanite, and rutile make up the accessory phases. Punctual rock cavities are filled with fluorite, muscovite, rutile, pyrochlore, illite, montmorillonite, pyromorphite, and helvite (for details on accessory phases, see Souza *et al.* 2020a).

This pegmatite also displays a younger minor intrusive unit constituted of euhedral amazonite and quartz crystals healed by cleavelandite, texturally distinct from the amazonite zone (Fig. 3C). The Serra Branca pegmatite presents two magmatic generations of amazonite, the former occurs within the main body, whereas the second is part of minor intrusive rocks, which usually presents a lighter color, besides the characteristic association with cleavelandite. Such distinction is strongly based on field relationship and chemical evidence (for details, see Lira Santos *et al.* 2020).

The albite zone is composed of saccharoidal white albite and grayish anhedral quartz with spessartine, ilmenite, zircon, columbite-(Mn), pyrochlore group minerals, fluorite, and



gahnite as accessory minerals (Fig. 3B). This zone is mainly located at the bottom of the pegmatite but sometimes penetrates the upper part of the body, and at the contact with the amazonite zone exhibits a major concentration of mafic minerals [e.g., ilmenite, magnetite, and columbite-(Mn)].

MATERIAL AND METHODS

All amazonite crystals used in this study were collected from the main body, the minor intrusive body, and the mine tailing from the Serra Branca amazonite pegmatite (for location and description of samples, see Suppl. Mat. S1).

Gemology

Standard gemological studies (e.g., refractometry, birefringence, and specific gravity) were carried out at the Gemology Laboratory of Universidade Federal de Pernambuco (LABGEM-UFPE) in amazonite samples prepared as ~1-mm-thick double-polished plates. A Schneider RF2 refractometer with a polarizing filter of 589.3 nm and a refractive index fluid ($n = 1.79$) was employed to measure the refractive index and birefringence. Weight and specific gravity from amazonite hand specimen samples were obtained by a Shimadzu AUY220 hydrostatic digital analytical balance, with a sensibility of 0.1 mg.

X-ray diffraction

The XRD analysis was performed in perthitic amazonite powder samples at the Laboratory of Mineral Technology of the Universidade Federal de Pernambuco, using a Bruker D2-Phaser diffractometer equipped with a Lynxeye one-dimensional detector, with monochromatic radiation of Cu-K α (30 kV, 10 mA; K α wavelength: 1.54060 Å); goniometer step of 0.0202°/s, counting time of 1.0 s, and 2 θ scanning from 4° to 80°.

Petrographic microscope BX51

Polished thin sections perpendicular to the (001) cleavage was selected to observe both Albite and Pericline twinning. A BX51 Olympus petrographic microscope was used, employing 1 \times to 50 \times objectives. An Olympus DP26 camera system from Olympus was used to register photomicrographs.

Laser ablation-inductively coupled plasma-mass spectrometry

The trace elements analysis of amazonite crystals collected at the transversal profile of the main body was performed by LA-ICP-MS using a double-focusing sector field mass spectrometer, model ELEMENT XR, from Thermo Scientific which is combined with the excimer-based NewWave UP193FX laser probe at the Geological Survey of Norway. The analyses were done on surface-polished 300- μ m-thick sections glued with Epoxy on standard glass slides (48 \times 28 \times 1.5 mm). The 193-nm laser had a repetition rate of 20 Hz, a spot size of 75 μ m, and an energy fluence of 5.5–6.5 mJ/cm² on the sample surface. External multistandard calibration was performed using the

reference materials NIST SRM 610, 612, and 614 and 1830, BAM No. 1 amorphous SiO₂ glass from the Federal Institute for Material Research and Testing in Germany. The Qz-Tu synthetic pure quartz monocrystal provided by Andreas Kronz from the Geowissenschaftliches Zentrum Göttingen (GZG), Germany. Certified, recommended, and proposed values for these reference materials were taken from Jochum *et al.* (2011).

Electron microprobe analyses

Major and trace elements were obtained with an electron probe microanalyzer (EPMA), model JXA-8230 from JEOL at the Electron Microprobe Laboratory (LASON) in the Geoscience Institute of Universidade de Brasília. The analyses were performed on 30- μ m-thin polished standard sections coated with carbon in an Edwards Auto 306 vacuum chamber. The probe system used LASON's internal multistandard calibration with the following reference materials: albite (Na), microcline (K), wollastonite (Si and Ca), topaz (F), vanadinite (V, Cl, and Pb), TiMnO₃ (Ti and Mn), andradite (Fe), forsterite (Mg), barite (Ba), pollucite (Cs), ZnS (Zn), apatite (P), CuFeS₂ (Cu), Cr₂O₃ (Cr), NiO (Ni), RbSi (Rb), and baddeleyite (Zr). Instrument conditions were acceleration voltage of 15 kV, an electric current of 10 nA, the electron beam diameter of 1 μ m, and a counting time of 10 s for each element peak. Backscattered electron images were used for selecting analysis spots and to avoid mineral inclusions.

Visible and infrared absorption and reflectance spectroscopies

For the spectroscopic analyses, the amazonite was prepared as double-polished plates with approximately 1 mm of thickness. The visible spectroscopy was recorded with a double-beam spectrometer model Perkin Elmer Lambda 35 at the Ionizing Radiation Metrology Laboratory, UFPE. The spectra were obtained in the most transparent region of each sample by delimiting the beam with a 3-mm diameter window. These spectra were obtained with a slit of 4 nm from 1,100 to 190 nm at 120 nm/min. Infrared spectra were measured with a Fourier Transform Infrared (FTIR) spectrometer model Bruker Vertex 70 in the Mineral Technology Laboratory (Mining Engineering Department, UFPE). The signals were recorded after 128 scans with a resolution of 4 cm⁻¹ from 7,500 to 1,500 cm⁻¹. Reflectance spectroscopy (RE) was conducted in the same 11 amazonite crystals, using FieldSpec4™ Standard Resolution spectroradiometer (Analytical Spectral Devices) at the Institute of Geosciences of the Universidade Estadual de Campinas (Unicamp). The spectroradiometer records spectra in 2,151 channels, with wavelengths ranging from 350 to 2,500 nm that comprise the visible to near-infrared range (VNIR, 350–1,200 nm) and the short-wave infrared range (SWIR, 1,200–2,500 nm). The spectral sampling is 1.4 nm for the 350–1,000 nm range and 1.1 nm for 1,001–2,500 nm (Malvern Panalytical 2018). A contact probe with an internal light source and ~20 mm spot size was used. Data were calibrated using a Spectralon® white plate. The samples

were measured at least three times, and an average reflectance curve was calculated for each sample.

RESULTS

Macroscopic description of the studied amazonite

The amazonite from the main body occurs as megacrysts up to 2 m long with subhedral to euhedral habits (Fig. 4A), exhibiting widespread fractures healed by saccharoidal albite and grayish quartz (Fig. 4B), while the amazonite from the minor intrusive unit appears as megacrysts up to 40 cm healed by prismatic albite (cleavelandite) and associated with smoky quartz. In general, the amazonite crystals are characterized by well-developed graphic intergrowths with quartz (Fig. 4C), macroscopic Carlsbad twinning, as well as anastomosed veins of perthitic intergrowth (Fig. 4D). They present blue-green color, perfect cleavage in (001), and a good cleavage in (010). In general, the amazonite is opaque to translucent, but double-polished plates exhibit transparent areas that allowed refractive index determination. The $n\alpha$ index varies from 1.520 to 1.521, the $n\beta$ was 1.521 to 1.526, and the $n\gamma$ ranges from 1.525 to 1.529, yielding a 0.007–0.008 birefringence.

XRD analysis

The powder diffraction patterns revealed that the Serra Branca amazonite is low microcline with low albite intergrowth (Fig. 5). Measurements of the triclinic unit cell parameters (Goldsmith and Laves 1954) show a high degree of Al/Si ordering with values between $0.97 > \Delta > 0.90$. Thus, from

the point of view of the XRD technique, our amazonite specimens correspond to triclinic crystals close to the low microcline variety.

Feldspar microtextures

Twinning

The first magmatic generation amazonite from the main body (AM-01 to AM-03) generally shows rectangular cross-hatched microtextures formed by $\pm A/P$ twinning, while the second magmatic generation amazonite from the minor intrusive body (AMZ-28D) is mainly formed by $\pm A$ twinning and larger homogeneous areas.

The main body specimens are diverse and display different sizes of crosshatched microtextures with minor preserved parquet microtextures where pristine areas are surrounded by a framework of pseudoperiodic $\pm A/P$ tartan twinning (Fig. 6A). The development of irrational twinning along with the P orientation and chessboard twinning can also be observed (Fig. 6B).

Coarsening process takes place in those specimens seen by large $\pm A$ twins that include fine twins with a needle tip of contrary sign (Fig. 6C). Such occurrence is correlated to the zigzag aspect that coarsened albite films gained when crossed by those albite twins. However, coalescence of finer \pm Albite and Pericline laws of same orientation variant results in homogeneous areas into the P twinning orientation (Fig. 6D).

The minor intrusive unit specimen (AMZ-28D) also displays a coarsening process marked by large polysynthetic $\pm A$ twinning that interconnects larger homogeneous regions in the P twinning orientation (Fig. 6E). This specimen has numerous coarsened zigzag albite films scattered throughout the samples correlated to albite twins of needle tip (Fig. 6F) and minor crosshatched patterns that occur with chessboard twinning.

Albite intergrowth

The Serra Branca amazonite specimens exhibit albite intergrowth in coarsened films and veins, which can be seen by both macroscopic and microscopic scales, classifying them as macropertthites. The vein displays pseudoperiodic polysynthetic $\pm A$ twinning, mostly running parallel to the $\sim (100)$ direction.

The Ab-rich intergrowth occurs in the main body amazonite (AM-01 to AM-03) as veins with a thickness of 0.7–7.6 mm and length of 0.25–16.3 mm (Fig. 7A) and as coarsened films with thickness between tens to thousands of micrometers (Fig. 7B). They also exhibit parallel veins oriented to $\sim (110)$ with 0.4 to 90.4 μm thickness connecting the main veins parallel to $\sim (100)$ forming intricate networks of anastomosing configurations. Subhedral to anhedral albite crystals with polysynthetic twinning present distinct elongations and 0.3×0.1 mm to 2.2×0.6 mm in size (Fig. 7C). The larger crystals are subhedral and have the larger prismatic face mostly oriented $\sim (1\bar{1}0)$ located in the $\pm A/P$ twinning mass, and the minors are anhedral and often associated with the perthitic veins.

The minor intrusive unit amazonite Ab-rich veins (AMZ-28B) are mostly oriented to $\sim (100)$, but sometimes exhibit a braid microtexture given by the connection between veins

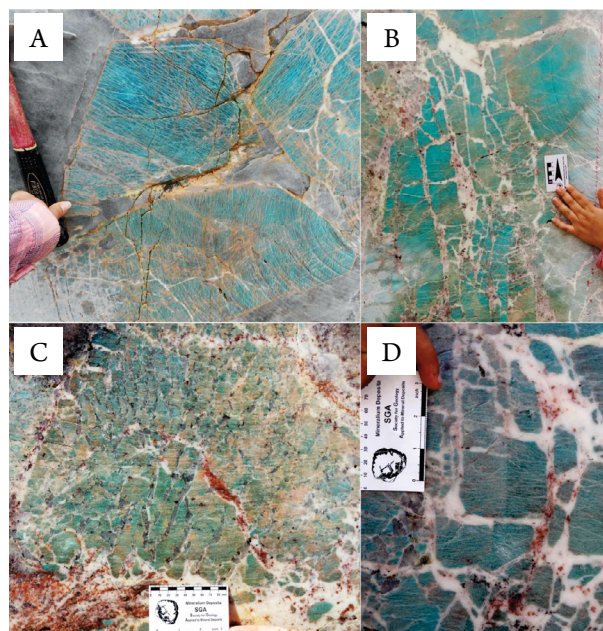


Figure 4. The Serra Branca amazonite: (A) Bluish green amazonite subhedral crystals surrounded by smoky quartz; (B) Fractured amazonite healed with saccharoidal white albite; (C) Graphic intergrowth between the bluish green amazonite and smoky quartz; (D) Macroscopic twinning in fractured perthitic bluish green amazonite healed by white saccharoidal albite.

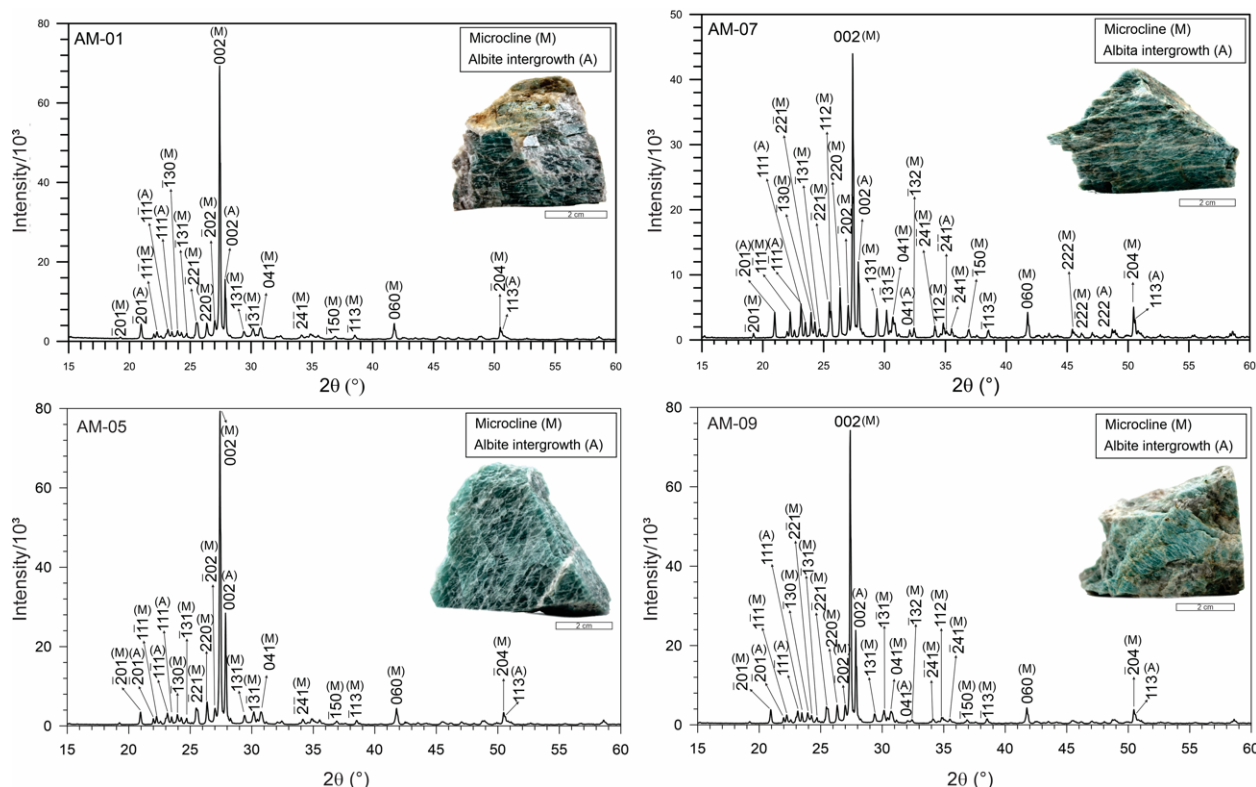


Figure 5. Representative diffractograms of amazonite crystals from Serra Branca pegmatite composed of the K-rich phase (microcline/amazonite) and the Na-rich phase (albite).

$\sim (11\bar{0})$ and the anastomosed veins $\sim (100)$. The veins $\sim (100)$ have thickness and length ranging from 0.2 to 6.6 mm and 3 to 15 mm, respectively. They also displayed veins running $\sim (010)$ with 140.8–313 mm in length and 0.8–7.5 mm in thickness (Fig. 7D), connecting the main veins at $\sim (100)$.

Mineral chemistry

The K-rich phase of the main body and minor intrusive unit amazonite has a modal composition of $Or_{95.32-93.03}Ab_{6.96-4.58}An_{0.18-0.02}$ and $Or_{95.24}Ab_{4.59}An_{0.18}$, respectively, while the intergrowth albite from both amazonite crystals is very close to that of the albite end-member with $Or_{1.38-0.33}Ab_{99.50-98.48}An_{0.47-0.08}$ (Tab. 1). Both amazonite magmatic generations have elevated contents of Rb, Pb, Ba, Fe, Cs, and Tl (Tab. 2).

The concentration of Rb varies from 7,575 to 4,838 ppm, being the most abundant minor element. Concentrations of Pb are moderate to high, ranging from 1,229 to 933 ppm. Barium contents are elevated from 260 to 430 ppm. Fe and Cs are also present with concentrations ranging from 417 to 633 ppm and 131 to 435 ppm, respectively. The albite intergrowth from both magmatic generations has elevated contents of Fe, Pb, Sr, and Ga, with 500–719 ppm for Fe, 76–161 ppm for Sr, 36–151 ppm for Pb, and 50–78 ppm for Ga, yet the minor intrusive unit albite exhibits a high content Rb (40.5 ppm). For detailed petrogenetic chemistry, see Lira Santos *et al.* (2020).

Spectroscopy

The absorption spectra in the VNIR for the double-polarized amazonite plates only showed a broad absorption band with maximum absorption at 616–620 nm (Fig. 8A). Spectra obtained by FTIR spectroscopy exhibited broad bands

with maximum absorption at 3,404–3,406 cm^{-1} , sharp bands at the range of 2,025–2,144 cm^{-1} , and subtle bands at 2,341–2,361 cm^{-1} (Fig. 8B).

The reflectance spectroscopy performed in the amazonite crystals at the VNIR showed bands with maximum absorption at 383–404 nm and bands centered at 633–640 nm (Fig. 8C). At the SWIR, absorption features centered at 1,410–1,416, 1,411–1,917, and 2,205–2,208 nm were observed. The AM-10 shows double absorption bands centered at 2,317 and 2,381 nm.

DISCUSSION

Twinning in the Serra Branca Amazonitic Microcline

A conspicuous schematic model for the evolutionary sequence of transformations in perthitic K-rich feldspar from granitic pegmatites was proposed by previous investigations of Sánchez-Muñoz *et al.* (2012). According to these authors, K-feldspars in granitic pegmatites can be developed from a sanidine ancestor by two unlike initial precursors (disordered or ordered) after the monoclinic to triclinic transformation. We interpret that the Serra Branca amazonite microtextures were developed via an avalanche-like event (Sánchez-Muñoz *et al.* 2008), consistent with an ordered precursor, with a low P content. Orthoclase was not observed in thin sections or XRD patterns as the initial precursor for twin recrystallizations; therefore, ordered microcline was formed directly from a sanidine ancestor, as the magmatic original phase.

The evolution path seen in both magmatic generations of the Serra Branca amazonitic microcline is the twin

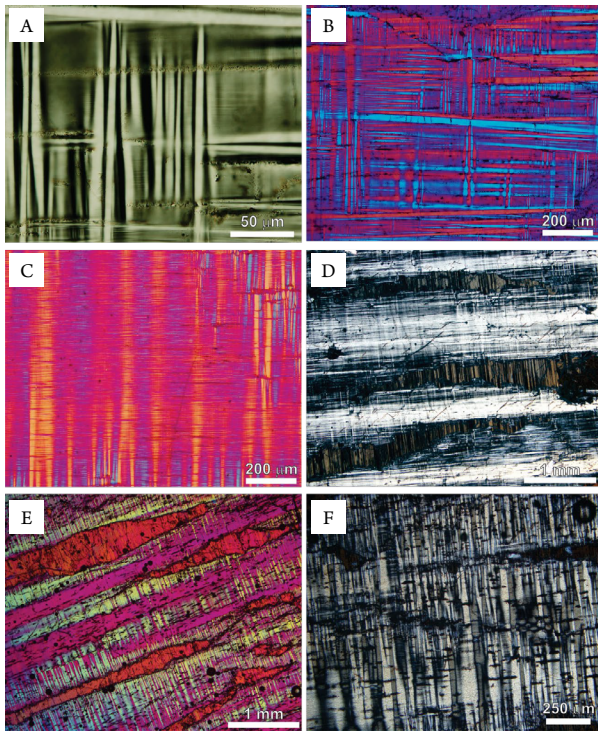


Figure 6. Optical micrographs perpendicular to (001) plane of twin patterns in the Serra Branca amazonite crystals: (A) Specimen AM-02 displaying the ordered precursor in quadrangular shape surrounded by A/P twins of tartan twinning; (B) Crosshatched pattern in the specimen AM-02, with red plate added, showing parquet, chessboard, and irrational twinning; (C) Finer twins coarsening to larger twins of specimen AM-03. Large albite including finer needle tip albite twins of contrary sign is seen in the top right of the image (red plate added). (D) Larger homogeneous areas (white bands) in the P twin orientation given by coalescence of finer \pm Albite and Pericline laws of same orientation variant from AM-01. (E) Amazonite from the minor intrusive unit with larger homogeneous regions in pink interconnected by \pm large polysynthetic A twinning (red plate added). (F) Specimen AMZ-28D displaying zigzag albite films together with large albite twins of needle tip.

coarsening. Figure 9 represents how the twinning process began into the Serra Branca amazonite, where except for the beginning, the scheme followed the one in Sánchez-Muñoz *et al.* (2012). The first step was the crystallization of albite crystals with the larger prismatic face oriented closely to $\sim (1\bar{1}0)$ (Fig. 9A), then the sanidine ancestor and subsequent Na, K exsolution was formed (Fig. 9B), which evolved to the ordered precursor (Fig. 9C) until the development of parquet twinning (Fig. 9D). As a result, the amazonite specimens displayed different stages of twinning generations distinguished in the evolutionary scheme according to Sánchez-Muñoz *et al.* (2012), which are discussed below.

Most of the twin microstructures that we have observed are transformations of the “fine and very fine \pm A/P twins” of the I-tg into “coarse \pm A twins” of the second generation of twins (II-tg). Thereby, the specimens from the main body have twinning patterns coherent to the I-tg and partial conversion of the I-tg into the II-tg, while the specimens from the minor intrusive unit show patterns similar to the II-tg.

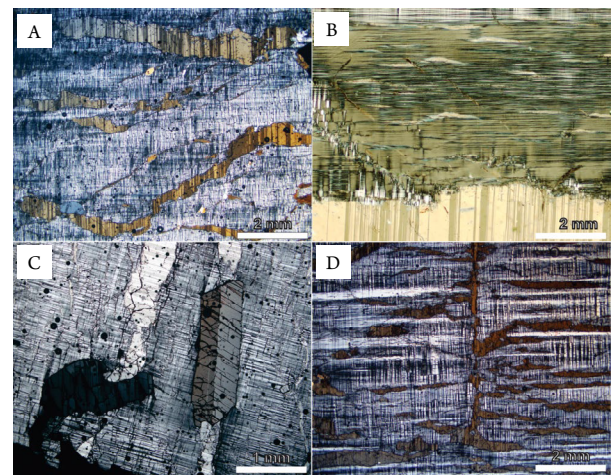


Figure 7. Optical micrographs perpendicular to (001) plane of albite intergrowth in the Serra Branca amazonite: (A) Perthitic amazonite (AM-01) with pseudoperiodic polysynthetic \pm A twinning albite veins in yellow color, mostly oriented parallel $\sim (100)$ and minor oriented $\sim (110)$; (B) Albite coarsened films (AM-03) with thickness between tens to hundreds of micrometers; (C) Albite crystals (AM-03) with pseudoperiodic polysynthetic \pm A twinning connected with the perthitic veins, which are oriented $\sim (100)$; (D) Albite perthitic vein in orange color oriented at $\sim (010)$, exhibiting pseudoperiodic polysynthetic \pm A twinning, connected to albite veins in $\sim (100)$ in the specimen AMZ-28D.

Therefore, as discussed by Sánchez-Muñoz *et al.* (2012) for I-tg where the twins developed initially by a high-temperature “dry” process, seems to be the case of the first magmatic generation amazonite, which also experimented a minor “wet” process responsible for the initial process of coarsening seen by large \pm A twins and homogeneous areas. On the other hand, the twinning of the second magmatic generation amazonite underwent the “wet” process related to postmagmatic aqueous fluid forming the large areas of coalescence of twins with different orientations but equal sign in the $\sim (010)$ direction.

Albite intergrowth microtextures

The Serra Branca amazonite displays Ab-rich (Ab_{99}) coarsened films and perthitic veins with orientations close to $\sim (010)$. Such intergrowths can be interpreted as starting with coarsened films that later evolve to the perthitic veins. In this way, the lamellae films were probably formed by Na-K interdiffusion initiated before the $C2/m$ to $C\bar{1}$ transformation and then coarsened during the microcline twinning due to fluids that had penetrated the crystal along misfit dislocations (Andersen 1928, Parsons *et al.* 2015).

The albite crystals in the Serra Branca amazonite can be correlated to two distinct formation events. The larger crystals were probably formed earlier in the pegmatite melt (Fig. 9A) since they are randomly scattered and mostly oriented close to $\sim [1\bar{1}0]$; a similar pattern is also seen in the amazonite crystals from Takami granitic pegmatite, Japan (Nakano and Makino 2010). The smaller crystals with no orientation, mainly located along the veins, were interpreted as subgrains correlated to the film-coarsening process as seen in the study by Lee and Parsons (2015).

Table 1. Major and minor elements in wt.% from the Serra Branca amazonite obtained by EPMA.

n	AMAZONITE				ALBITE			
	AM-01	AM-02	AM-03	AMZ-28D	AM-01	AM-02	AM-03	AMZ-28D
	11	11	12	12	1	1	1	1
SiO ₂ (wt. %)	64.96	66.39	65.52	64.42	68.46	69.01	69.86	68.60
TiO ₂	0.02	0.04	0.04	0.01	0.07	–	0.09	–
Al ₂ O ₃	16.84	16.69	16.59	16.76	17.85	17.90	17.72	17.39
FeO	0.07	0.05	0.06	0.05	0.07	0.15	0.09	0.06
CaO	0.01	–	0.01	0.03	0.04	0.09	0.05	0.10
Na ₂ O	0.68	0.76	0.55	0.49	11.78	11.69	11.68	11.26
K ₂ O	14.91	15.47	15.45	15.37	0.06	0.10	0.06	0.10
BaO	0.02	0.05	0.03	0.02	0.11	–	0.05	–
P ₂ O ₅	–	0.01	0.02	0.02	–	0.04	–	–
PbO	0.11	0.12	0.14	0.10	0.19	–	0.06	–
Cs ₂ O	0.06	0.10	0.04	0.07	0.13	0.14	–	–
Rb ₂ O	1.16	0.77	1.10	0.61	–	–	–	–
Total	98.84	100.45	99.55	97.75	98.77	99.11	99.64	97.51
T site								
Si (<i>apfu</i>)	3.05	3.06	3.06	3.05	3.04	3.04	3.06	3.04
Al	0.93	0.91	0.91	0.93	0.93	0.93	0.91	0.94
Total	3.98	3.97	3.97	3.98	3.97	3.97	3.97	3.98
M site								
K (<i>apfu</i>)	0.84	0.87	0.92	0.93	0	0.01	0	0.01
Na	0.12	0.1	0.05	0.04	1.01	1	0.99	0.99
Rb	0.03	0.02	0.03	0.02	0	0	0	0
Total	0.99	0.99	1	0.99	1.01	1.01	0.99	1
Or, mol. %	93.43	93.03	94.76	95.24	0.33	0.54	0.33	1.38
Ab	6.5	6.96	5.16	4.59	99.48	99.07	99.5	98.48
An	0.08	0.02	0.07	0.18	0.18	0.4	0.18	0.14

n: number of analyses; *apfu*: atoms per formula unit. AM-01 to AM-03 correspond to the first magmatic generation, and AMZ-28D corresponds to the second magmatic generation. Oxygen base number = 32.

Table 2. Trace elements in ppm from the Serra Branca amazonite obtained by LA-ICP-MS.

		AMAZONITE				ALBITE			
		AM-01	AM-02	AM-03	AMZ-28D	AM-01	AM-02	AM-03	AMZ-28D
LOD									
0.1	Li (ppm)	2.65	2.90	2.90	11.65	0.09	0.33	0.14	0.54
0.05	Ge	10.85	9.75	6.35	9.35	10.86	9.54	5.62	5.54
0.01	Rb	7,574.70	7,167.35	4,940.80	5,083.35	0.86	0.92	0.61	40.50
2.9	Sr	310.45	417.30	390.05	79.00	161.54	108.94	76.15	117.51
0	Cs	434.90	413.40	180.40	182.50	0.39	0.49	0.06	0.77
0.28	Ba	260.95	263.75	430.60	10.70	3.45	1.48	1.01	10.68
0	Tl	107.90	101.85	70.05	52.50	0.20	0.05	0.05	0.33
0.45	Pb	933.25	869.80	1,123.75	1,028.15	151.37	79.95	92.89	35.89
2.3	P	14.25	12.60	14.95	12.00	9.04	9.84	12.11	12.91
2.8	Fe	633.50	594.25	549.00	417.20	686.75	719.23	548.98	500.42
0.02	Ga	84.75	77.80	59.60	93.65	72.67	77.86	50.08	65.19
0	Y	0.01	0.01	b.d.	0.01	0.06	b.d.	b.d.	0.14
0.01	La	0.09	0.08	0.16	0.54	0.06	b.d.	0.02	0.04
0	Ce	0.07	0.06	0.1	0.13	0.07	0.01	0.01	0.03
0	Eu	0.15	0.18	0.26	0.24	0.09	0.04	0.03	0.03

LOD: limit of detection, b.d.: below detection limits. AM-01 to AM-03 correspond to the first generation, and AMZ-28D corresponds to the second generation. Source: adapted from Lira Santos *et al.* (2020).

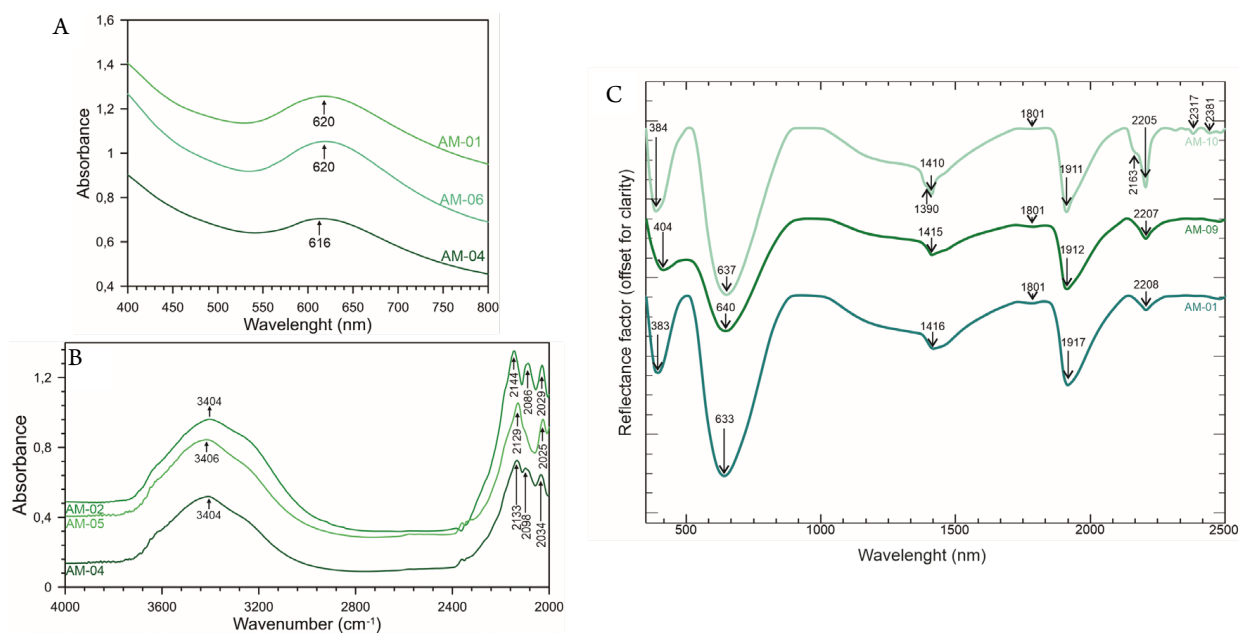


Figure 8. VNIR and FTIR absorption and reflectance spectra of representative Serra Branca amazonite crystals: (A) VNIR spectra with absorption bands centered at 616–620 nm. (B) FTIR absorption spectra with broad absorption band centered at 3,404–3,406 cm^{-1} and some subtle absorption bands between 2,144 and 2,025 cm^{-1} ; (C) Stacked reflectance spectra of representative Serra Branca amazonite grain samples. Average of three spectral analyses for samples AM-01, AM-09, and AM-10.

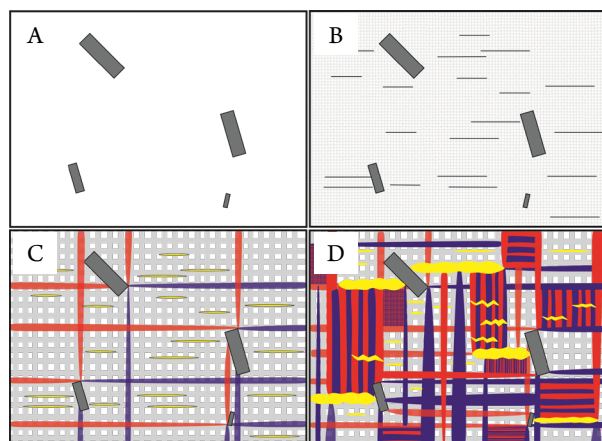


Figure 9. Microtextural scheme of microcline for the first generation of $\pm A/P$ fine twins (in gray color) and the second generation of $\pm A$ coarse twins (in red/blue colors) in amazonite from the Serra Branca pegmatite, based on the model developed in [14]. (A) Sanidine ancestor with $C2/m$ symmetry and albite crystal as inclusions. (B) Fine $\pm A/P$ twinning from the monoclinic-triclinic transformation as the initially ordered precursor, with additional development of fine albite exsolution films. (C) Initial coarsening of the $\pm A/P$ twins as the I-tg observed at the optical scale, with some coarsened albite films. (D) Development of coarse II-tg mainly along $\pm A$ twinning, developed from the interface with albite veins, and the development of serrated boundaries in coarsened albite films, associated with deformational twinning.

Trace elements partitioning in the Serra Branca Amazonite

The high contents on Rb (4,941–7,575 ppm), Pb (870–1,028 ppm), Sr (79–417 ppm), Ba (11–431 ppm), Cs (181–435 ppm), Fe (417–633 ppm), and Ga (60–94 ppm) of the Serra Branca amazonite are compatible with evolved NYF

pegmatites (Sokolov 2006, Lira Santos *et al.* 2020). The Serra Branca amazonite displays two generations of magmatic crystallization, where the first one (main body amazonite) shows strong partitioning of the elements Rb, Cs, Sr, Ba, Tl, and Pb into the potassic phase. The second magmatic generation (minor intrusive unit amazonite) displays a similar manner with elevated partitioning of Rb, Cs, Tl, Pb, and minor Li. The main difference between them is the Sr behavior. The second magmatic generation amazonite also displays similar values of Ba and P between both potassic and sodic phases. Iron and Ga usually substitute Si or Al in the T site, and they have similar amounts for the K-rich and Na phases in both amazonite magmatic generations. The rare earth elements concentrations are typically low in the K-feldspars, and in the Serra Branca amazonite, they show partitioning into the potassic phase that is enriched in La, Ce, and Eu.

Lira Santos *et al.* (2020) indicated that the forming melt for the amazonite and albite zones is the same, which could explain the Pb not only occurring in elevated values in the potassic phase but also contributing to the sodic compositions. Hence, fluids responsible for the coarsening events that generated the large albitic veins can be expected to belong to the albite zone. Therefore, one must consider that the amazonite bulk composition probably changed since the albite veins formation occurred due to fluids present in the coarsening event.

Spectroscopic features in the Serra Branca Amazonite: color and water presence

Several papers have discussed the amazonite coloring and its spectroscopic characteristics (Hofmeister and Rossman 1985, Julg 1988, Petrov 1993, Ostrooumov and Banerjee 2005, Ostrooumov 2012, Ostrooumov 2016). The most accepted hypothesis for the blue-green color relates to structural

incorporation of Pb in the alkali sites as well as structural vacancies largely occupied by H₂O, a possible catalyst (Hofmeister and Rossman 1985). In contrast, Vokhmentsev *et al.* (1989), Ostrooumov and Banerjee (2005), and Ostrooumov (2016) proposed five models of colors center in amazonite, which are related to the exchange-coupled complex (Pb⁺–[O, OH]–Fe³⁺), and/or Pb⁺ electron hole center in oxygen (O[–]Pb⁺), also by finely dispersed oxides and hydroxides of Fe, the hole center (Al–O[–]Al), and structural center ^{IV}Fe³⁺.

In this way, the sharp bands in the Serra Branca amazonite with peaks at 383–404 nm can be related to 380 nm observation in amazonite crystals from Keivy granitic pegmatite (Russia; Ostrooumov and Banerjee 2005), which according to these authors resulted by finely dispersed oxides and hydroxides of Fe, the hole center (Al–O[–]Al) and structural center ^{IV}Fe³⁺. The studied amazonite crystals presented absorption bands correlated to the bluish green color in the VNIR spectra at 616–620 nm and in the reflectance spectroscopy spectra centered at 633–640 nm, allowing us to interpret the presence of Pb impurities corroborating the hypothesis previously discussed.

Alkali feldspar minerals are usually dehydrated, but the presence of water is relatively common, especially in amazonite (Hofmeister and Rossman 1985, Beran 1986, Nakano *et al.* 2001, Ostrooumov 2016, Lira Santos *et al.* 2017). Water plays an important role in the blue-green color of amazonites, in the process of forming coarse perthites, and as catalysts for the formation of microcline twins (Brown and Parsons 1984, Hofmeister and Rossman 1985, Smith and Brown 1988, Sánchez-Muñoz *et al.* 2008). Absorption bands related to the presence of water and the vibrational modes of the H₂O molecule for amazonite crystals are often centered at 3,200, 3,420, 3,440, 3,420, 3,550, 3,622, and 3,698 cm^{–1} (Hofmeister and Rossman 1985, Ostrooumov 2016). Broad bands with maximum absorption at 3,404–3,406 cm^{–1} were observed, showing the presence of water in the Serra Branca amazonite crystals. In addition, absorption bands near 1,410–1,416 and 1,411–1,917 nm in the reflectance spectra corroborate with the bands seen in the infrared absorption spectra, also indicating the presence of water on this K-feldspar.

The subtle absorption bands centered at 2,317 and 2,381 nm in the amazonite can be explained by the alteration of the K-feldspar to kaolinite, which exhibits doublet features near 2,300 nm caused by the OH-stretch mode (Hunt 1977). Other sharp bands at the range of 2,025–2,144 cm^{–1} in the infrared absorption spectra are possibly due to silicon-oxygen stretching fundamentals modes of vibration.

CONCLUSIONS

The Serra Branca pegmatite is an extraordinary rock with valuable bluish green amazonite crystals, formed by an intergrowth of low albite and low microcline XRD varieties, having micropertthitic textures with albite films, as well as macropertthitic textures with albite veins, and also I-tg and II-tg twin microstructures. It occurs as subhedral to euhedral megacrysts

exhibiting graphic intergrowth with grayish quartz, mesoscopic Carlsbad growth twinning. Two magmatic generations are distinguished into the amazonite phases, and both exhibited an evolution following twin coarsening. The first magmatic generation amazonite displayed I-tg, which is formed from the monoclinic to triclinic transformation giving rise to an initially ordered precursor, formed by $\pm A/P$ twins. This original microstructure was transformed by the II-tg through a coarsening process, giving rise to $\pm A$ twinning, mostly seen by the second magmatic generation amazonite. Irrational twinning also occurred in the II-tg, a phenomenon that is indicative of an anorogenic origin for the amazonite pegmatite (Sánchez-Muñoz *et al.* 2017).

The Serra Branca amazonite shows high concentrations of Rb, Pb, Sr, Ba, Cs, Fe, and Ga, evidencing the evolved aspect of the Serra Branca amazonite pegmatite. The Pb presence is responsible for the blue-green color as shown by its characteristic absorption spectra centered mainly at 616–640 nm. The presence of water is also displayed by the 3,404–3,406 cm^{–1} broad bands at the FTIR spectroscopy, as well as by 1,410–1,416 and 1,411–1,917 nm bands at the reflectance spectroscopy.

The microtextural, microstructural, and spectroscopic characteristics of the Serra Branca amazonite demonstrate that the twinning process did not destroy the color of amazonite in the subsolidus stage, as the coarsening of albite films into albite veins did. In twinning, the color can be destroyed by the intense recrystallization of the crystal structure, especially when a strong II-tg and III-tg occur, where K-feldspars become normally white because of the exit of the chemical impurities in their color centers (Sánchez-Muñoz *et al.* 2012). In the case of the Serra Branca amazonite, which presents the II-tg and has the Pb as the main cause of the color, the amazonite was crystallized as magmatic sanidine, and subsequent transformation into microcline preserved the original blue-green color rather than destroying it.

ACKNOWLEDGMENTS

The authors are grateful to the Granistone S/A company for their support during fieldwork and the collecting of samples in Vieirópolis and to Mr. Antônio Braga for his logistical support during visits to the area. The authors also thank Prof. Pedro Guzzo of the Mineral Technology Laboratory in the Universidade Federal de Pernambuco (UFPE), Prof. Axel Muller of Natural History Museum from Oslo and London, and Prof. Nilson Botelho of the Electron Microprobe Laboratory in the Geoscience Institute of Universidade de Brasília. The authors are grateful to Prof. Dr. Carlos R. de Souza Filho, Dr. Rebecca Scafutto, Dr. Rosa Pabón, and Prof. Dr. Thais Carrino for the reflectance spectroscopy, done in the Institute of Geosciences of Unicamp. We thank the Coordenação de Aperfeiçoamento de Pessoal de Nível Superior (CAPES) for the scholarship granted to Glenda Lira Santos, Igor Manoel Belo de Albuquerque e Souza, and José Ferreira de Araújo Neto during this research.

ARTICLE INFORMATION

Manuscript ID: 20210072. Received on: 28 SEP 2021. Approved on: 16 MAY 2022.

How to cite this article: Santos G.L., Barreto S.B., Souza I.M.B.A., Araújo Neto J.F., Sánchez-Muñoz L., Santos L.C.M.L. Microtextural, spectroscopic, and chemical characterization of amazonite from the Serra Branca Pegmatite, Northeastern Brazil. *Brazilian Journal of Geology*, 52(3):e20210072. <https://doi.org/10.1590/2317-488920220210072>.

G.L.S., S.B.B.: Conceptualization, data curation, formal analysis, investigation, methodology, project administration, resources, supervision, validation, visualization, writing — original draft, writing — review & editing. I.M.B.A.S., J.F.A.N.: Data curation, methodology, validation, visualization, writing — original draft, writing — review & editing.: L.S.M.: Conceptualization, formal analysis, investigation, methodology, supervision, validation, visualization, writing — original draft, Writing — review & editing. L.C.M.L.S.: Data curation, validation, visualization, writing — original draft, writing — review & editing.

Competing interests: the authors declare no competing interests.

REFERENCES

- Abad-Ortega M.D.M., Hach-Ali P.F., Martin-Ramos J.D., Ortega-Huertás M. 1993. The feldspars of the Sierra Albarrana granitic pegmatites, Córdoba, Spain. *The Canadian Mineralogist*, 31(1):185-202.
- Alfonso P., Melgarejo J.C., Yusta I., Velasco F. 2003. Geochemistry of the feldspars and muscovite in granitic pegmatite from the Cap the Creus Field, Catalonia, Spain. *The Canadian Mineralogist*, 41(1):103-116. <https://doi.org/10.2113/gscanmin.41.1.103>
- Almeida F.F.M., Hashui Y., Brito Neves B.B., Fuck R.A. 1981. Brazilian structural provinces: an introduction. *Earth-Sciences Reviews*, 17(1-2):1-29. [https://doi.org/10.1016/0012-8252\(81\)90003-9](https://doi.org/10.1016/0012-8252(81)90003-9)
- Andersen O. 1928. The genesis of some types of feldspar from granite pegmatites. *Norske Geologisk Tidsskrift*, 10(1-2):116-207.
- Araújo Neto J.F., Lira Santos G., Souza I.M.B.A., Barreto S.B., Santos L.C.M.L., Bezerra J.P.S., Carrino T.A. 2018. Integration of remote sensing, airborne geophysics and structural analysis to geological mapping: a case study of the Vieirópolis region, Borborema Province, NE Brazil. *Geologia USP. Série Científica*, 18(3):89-103. <https://doi.org/10.11606/issn.2316-9095.v18-140834>
- Barreto S.B. 1991. *Caracterização químico-mineralógica dos berilos de Tenente Ananias* – RN. PhD Thesis, Universidade Federal de Pernambuco, Recife, 219 p.
- Beran A. 1986. A model of water allocation in Alkali Feldspar, derived from Infrared-Spectroscopic investigations. *Physical and Chemical Minerals*, 13(5):306-310. <https://doi.org/10.1007/BF00308347>
- Bruto Neves B.B., Fuck R.A., Pimentel M.M. 2014. The Brasiliano collage in South America: a review. *Brazilian Journal of Geology*, 44(3):493-518. <https://doi.org/10.5327/Z2317-4889201400030010>
- Brown J.A., Martins T., Černý P. 2017. The Tanco pegmatite at Bernic Lake, Manitoba. XVII. Mineralogy and Geochemistry of Alkali Feldspars. *The Canadian Mineralogist*, 55(3):483-500. <https://doi.org/10.3749/canmin.1700008>
- Brown W.L., Parsons I. 1984. The nature of potassium feldspar, exsolution microtextures and development of dislocations as a function of composition in perthitic alkali feldspars. *Contributions to Mineralogy and Petrology*, 86(4):335-341. https://ui.adsabs.harvard.edu/link_gateway/1984CoMP...86..335B/doi:10.1007/BF01187138
- Foord E.E., Martin R.F. 1979. Amazonite from the Pikes Peak Batholith. *The Mineralogy Record*, 10(6):373-384.
- Goldsmith J.R., Laves F. 1954. The microcline-sanidine stability relations. *Geochimica et Cosmochimica Acta*, 5(1):1-19. [https://doi.org/10.1016/0016-7037\(54\)90058-7](https://doi.org/10.1016/0016-7037(54)90058-7)
- Hofmeister A.M., Rossman G.R. 1985. A spectroscopic study of irradiation coloring of amazonite: structurally hydrous, Pb-bearing feldspar. *American Mineralogist*, 70(7-8):794-804.
- Hunt G.R. 1977. Spectral signatures of particulate minerals in the visible and near infrared. *Geophysics*, 42(3):501-513. <https://doi.org/10.1190/1.1440721>
- Jochum K.P., Weiss U., Stoll B., Kuzmin D., Yang Q., Raczek I., Jacob D.E., Stracke A., Birbaum K., Frick D.A., Günther D., Enzweiler J. 2011. Determination of reference values for NIST SRM 610-617 glasses following ISO guidelines. *Geostandards and Geoanalytical Research*, 35(4):397-429. <https://doi.org/10.1111/j.1751-908X.2011.00120.x>
- Julg A. 1998. A theoretical study of the absorption spectra of Pb²⁺ and Pb³⁺ in site K⁺ of microcline: application to the color of amazonite. *Physics and Chemistry of Minerals*, 25(3):229-233. <https://doi.org/10.1007/s002690050108>
- Larsen R.B. 2002. The distribution of rare-earth elements in K-feldspar as an indicator of petrogenetic processes in granitic pegmatites: Examples from two pegmatite fields in southern Norway. *The Canadian Mineralogist*, 40(1):137-152. <https://doi.org/10.2113/gscanmin.40.1.137>
- Lee M.R., Parsons I. 2015. Diffusion-controlled and replacement microtextures in alkali feldspars from two pegmatites: Perth, Ontario and Keystone, South Dakota. *Mineralogical Magazine*, 79(7):1711-1735. <https://doi.org/10.1180/minmag.2015.079.7.21>
- Lira Santos G., Souza I.M.B.A., Barreto S.B., Araújo Neto J.F., Müller A. 2020. The Serra Branca amazonite pegmatite field, Paraíba, Brazil – A new and unusual megacrystic amazonite deposit. *The Canadian Mineralogist*, 58(6):679-702. <https://doi.org/10.3749/canmin.1900095>
- Lira Santos G., Watanabe E.T.F., Araújo Neto J.F., Souza I.M.B.A., Barreto S.B. 2017. Mineralogical characterization of amazonites from Serra do Pinheiro, Sertânia (PE), Brazil. *Estudos Geológicos*, 27(1):95-107. <https://doi.org/10.18190/1980-8208/estudosgeologicos.v27n1p95-107>
- Malvern Analytical. 2018. ASD FieldSpec 4 Standard-Res Spectroradiometer. Available at: <https://www.asdi.com/products-and-services/fieldspec-spectroradiometers/fieldspec-4-standard-res/>. Accessed on: Aug. 1, 2022.
- Martin R.F., De Vito C., Pezzota F. 2008. Why is amazonitic K-feldspar an earmark of NYF-type granitic pegmatites? Clues from hybrid pegmatites in Madagascar. *American Mineralogist*, 93(2-3):263-269. <https://doi.org/10.2138/am.2008.2595>
- Medeiros V.C., Nascimento M.A.L., Galindo A.C., Dantas E.L. 2012. Augén gnáisses ríacianos no Domínio Rio Piranhas-Seridó – Província Borborema, Nordeste do Brasil. *Geologia USP. Série Científica*, 12(2):3-14. <https://doi.org/10.5327/Z1519-874X2012000200001>
- Nakano S., Makino K. 2010. Amazonitic alkali feldspar from the Tanakami Granitic pegmatite, southwest Japan. *Journal of Mineralogical and Petrological Sciences*, 105(2):45-56. <https://doi.org/10.2465/jmps.090301>
- Nakano S., Makino K., Eriguchi T. 2001. Microtexture and water content of alkali feldspar by Fourier-transform infrared microspectroscopy. *Mineralogical Magazine*, 65(5):675-683. <https://doi.org/10.1180/002646101317018497>
- Ostrooumov M. 2012. Algunas consideraciones mineralógicas y geoquímicas sobre la amazonita del estado de Chihuahua, México. *Revista Mexicana de Ciencias Geológicas*, 29(1):221-232.
- Ostrooumov M. 2016. *Amazonite: mineralogy, crystal chemistry, and typomorphism*. Amsterdam: Elsevier, 214 p.
- Ostrooumov M., Banerjee A. 2005. Typomorphic features of amazonitic K-feldspar from the Keivy granitic pegmatite (Kola Peninsula, Russia). *Schweizerische Mineralogische und Petrographische Mitteilungen*, 85:89-102. <https://doi.org/10.5169/seals-1655>

- Parsons I., Fitz Gerald J.D., Lee M.R. 2015. Routine characterization and interpretation of complex alkali feldspar intergrowths. *American Mineralogist*, **100**(5-6):1277-1303. <https://doi.org/10.2138/am-2015-5094>
- Petrov I., Mineva R.M., Bershov L.V., Agel A. 1993. EPR of [Pb-Pb]³⁺ mixed valence pairs in amazonite-type microcline. *American Mineralogist*, **78**(5-6):500-510.
- Prado F.S., Oliveira A.A., Leite E.A., Gomes F.E., Silva F.P., Colares J.Q.S. 1980. *Projeto Lavras da Mangabeira*: mapa geológico integrado (escala 1:200.000). Fortaleza: DNP/CPRM.
- Sánchez-Muñoz L., García-Guinea J., Beny J., Rouer O., Campos R., Sanz J., Moura O.J.M. 2008. Mineral self-organization during the orthoclase-microcline transformation in a granite pegmatite. *European Journal of Mineralogy*, **20**(4):439-446. <https://doi.org/10.1127/0935-1221/2008/0020-1844>
- Sánchez-Muñoz L., García-Guinea J., Zagorsky V.Y., Juwono T., Modreski P.J., Cremades A., Van Tandeloo G., Moura O.J.M. 2012. The evolution of twin patterns in perthitic K-feldspar from granitic pegmatites. *The Canadian Mineralogist*, **50**(4):989-1024. <https://doi.org/10.3749/canmin.50.4.989>
- Sánchez-Muñoz L., Muller A., Andrés S.L., Martin R.F., Modreski P.J., Moura O.J.M. 2017. The P-Fe diagram for K-feldspars: A preliminary approach in the discrimination of pegmatites. *Lithos*, **272-273**:116-127. <https://doi.org/10.1016/j.lithos.2016.10.030>
- Santos E.J., Souza Neto J.A., Silva M.R.R., Beurlen H., Cavalcanti J.A.D., Silva M.G., Dias V.M., Costa A.F., Santos L.C.M.L., Santos R.B. 2014. Metalogênese das porções norte e central da Província Borborema. In: Silva M.G., Rocha Neto M.B., Jost H., Kuyumjian R.M. (eds.). *Metalogênese das províncias tectônicas brasileiras* (p. 343-388). Belo Horizonte: CPRM.
- Smith J.V., Brown W.L. 1988. *Feldspar minerals*. 2nd ed. New York: Springer, 828 p.
- Sokolov M. 2006. *Characterization of Pb and selected trace elements in amazonitic K-feldspar*. PhD Thesis, McGill University, Montreal, Canada, 91 p.
- Souza I.M.B.A., Barreto S.B., Lira Santos G., Araújo Neto J.F., Guimarães I.P. 2020a. A mineralogia acessória do Amazonita Pegmatito Serra Branca: classificação de um pegmatito NYF na Província Borborema, Nordeste do Brasil. *Geologia USP. Série Científica*, **20**(3):47-61. <https://doi.org/10.11606/issn.2316-9095.v20-162199>
- Souza I.M.B.A., Guimarães I.P., Barreto S.B., Lira Santos G., Araújo Neto J.F. 2020b. Whole-rock and mineral chemistry characterization of contrasting granitoids, constraints on the source of the Vieirópolis NYF-type pegmatites, Northeastern Brazil. *Brazilian Journal of Geology*, **50**(2):1-23. <https://doi.org/10.1590/2317-4889202020190083>
- Souza Z.S., Martin H., Peucat J.-J., Jardim de Sá E.F., Macedo M.H.F. 2007. Calc-alkaline magmatism at the Archean-Proterozoic transition: the Caicó Complex Basement (NE Brazil). *Journal of Petrology*, **48**(11):2149-2185. <https://doi.org/10.1093/ptrology/egm055>
- Van Schmus W.R., Oliveira E.P., Silva Filho A.F., Toteu S.F., Penaye J., Guimarães I.P. 2008. Proterozoic links between the Borborema Province, NE Brazil, and the Central African Fold Belt. *Geological Society, London, Special Publications*, **294**:69-99. <https://doi.org/10.1144/SP294.5>
- Vokhmentsev A.Y., Ostrooumov M.N., Marin Y.B., Platonov A.N., Popov V.A., Tarashchan A.N., Shmakin B.M. 1989. *Amazonite*. Moscow: Nedra Publishing House, 192 p.
- Witzke T., Wegner R., Doering T., Pöllmann H., Schuckmann W. 2000. Serrabrancaite, MnPO₄·H₂O, a new mineral from the Alto Serra Branca pegmatite, Pedra Lavrada, Paraíba, Brazil. *American Mineralogist*, **85**(5-6):847-849. <https://doi.org/10.2138/am-2000-5-627>